Journal of Materials and Electronic Devices 4 (2023) 30-36


# Effect of the sintering temperature on the microstructure of MgB2 bulks manufactured by in-situ technique

Özlem Çiçek[1*], Kübra Yakıncı[1]

[1]Iskenderun Technical University, Faculty of Engineering and Natural Science, Department of Engineering Basic Sciences, Iskenderun, Hatay, Turkey

Besides many interesting features of $MgB_2$, it is important for the green economy of the future that it allows systems that use L-Ne or L-$H_2$ instead of cryogens; meanwhile as a light material, it can attract attention in terms of portable applications and especially space applications. $MgB_2$ bulks and wires are produced by various processing techniques that can be categorized as either in-situ or ex-situ methods. Both have their own advantages and disadvantages. Therefore, the decision on which method to use should be evaluated according to the needs of the application. For the good inter-grain connectivity, in-situ production should be chosen but improved. Instead of high temperatures and long heat treatment duration, examining the effect of relatively lower and shorter times on the material was deemed necessary for the optimization of the in-situ method.

For this reason, in this study, microstructural examination of bulk $MgB_2$ samples produced by in-situ method at 625, 650 and 700 °C for 6 and 12 hours, was carried out. The samples microstructural properties were investigated by XRD and SEM measurements. XRD measurements were performed between 20° and 80° with step size of 0.02° from the pellet surface. The crystallographic refinement was simulated using the Full Prof software by the Rietveld method. Lattice parameter and cell volume, phase fractions were determined. The crystallite size is calculated from the XRD results using the Debye-Scherrer formula. Magnetic $T_{c,mag}$ was determined as around 38,5 °K from the magnetization measurement. The results provide guideline for further optimization of the microstructure of bulk $MgB_2$ with enhanced properties.

***Keywords:*** *$MgB_2$, sintering temperature, Reitveld method*

*Submission Date: 17 August 2023*
*Acceptance Date: 13 September 2023*

**Corresponding author: ozlemthecicek@gmail.com*

## 1. Introduction

Superconducting materials lose their electrical resistance when cooled below their critical temperature, called Tc. Although the superconductivity properties of many elements, alloys, ceramics and compounds have been proven and established throughout history, only a limited number of materials have found a place in applications. For example, the superconductors most commonly considered to improve their properties in magnet and coil applications are Nb3Sn, NbTi, BSCCO, YBCO wires and tapes. Since magnesium diboride ($MgB_2$) was reported to be a metallic superconductor by "Prof. J. Akimitsu" [1] in 2001, much work has been done to improve the $MgB_2$ parameters through processing modification to make them suitable for applications as well [2-6]. $MgB_2$ superconductor's the ability to capture larger magnetic fields than conventional ferromagnets, grain boundaries act as pinning centers instead of weak bonds, simple chemical structure, easy production and low chemical cost compared to others, the ability to work as a multi-crystal without having to be a single crystal, ability to be produced in different shapes and sizes (such as

tube, strip, disc, cylinder, ring) [7-8]; making it an interesting superconductor for applications such as MRI [9-11], FCL, SQUIDs [12-14], motors, generators, etc. In addition, thanks to the transition temperature of 39 K, $MgB_2$-based technologies allow systems that use liquid Ne or liquid $H_2$ instead of cryogens as coolants [15-16]. $MgB_2$ is a lightweight material, making it a valuable superconductor, especially in portable applications, space applications, transportation, medicine, energy and other fields requiring low-mass materials [17]. For many of these applications, well-developed $MgB_2$ wires/cables/strips are needed, which have enormous potential for the development of the green economy of the future. Different production methods have been proposed to improve the transport properties of $MgB_2$ wires/cables/strips and basically these methods can be categorized as “in-situ” or “ex-situ” methods. Both methods have their own advantages and disadvantages. Therefore, the decision on "in-situ" or "ex-situ" production should be evaluated according to the needs of the application. Intergranular bonding is important for magnet applications. Therefore, "in-situ" production should be selected but developed.

As an alternative to the high temperatures and long heat treatment durations applied in the "in-situ" method, which makes production difficult and increases the cost, it was deemed necessary to examine the effect of relatively lower and shorter times on the material for the optimization of this method. Therefore, in this study, microstructural examination of bulk $MgB_2$ samples subjected to in situ heat treatment at 625, 650 and 700°C for 6 and 12 hours was carried out.

## 2. Experimental

The samples used in this study were prepared from powder mixtures with the same stoichiometric ratios (Mg:B=2:1). High purity Pavezyum Nano Amorphous Boron powder and Pavezyum Magnesium powder were used as starting materials by “in-situ” process in which the powders were first mixed and then subjected to heat treatment, Table 1. The powders were ground in an agate mortar and mixed homogeneously. These mixtures were then placed into pressing mold with a special shape, ensuring a homogeneous powder distribution, and pressed under 100 MPa. The pressed samples were subjected to heat treatment (HT) under Ar atmosphere at 625, 650 and 700 °C for 6 and 12 hours at each temperature value, and were left to cool in the furnace at the end of the heat treatment. The prepared samples were named 625-06, 625-12, 650-06, 650-12, 700-06 and 700-12. The first part of the code refers to the HT temperature, and the second part refers to the HT duration.

X-ray diffraction (XRD) and scanning electron microscopy (SEM) measurements were used to bring to light the microstructural features of all samples. XRD analyzes were performed using the Rigaku powder diffractometer system and Cu-Kα radiation. The produced bulk was scanned from the surface of pieces cut in equal sizes from $MgB_2$ samples between 20° and 80° with an angular step of 0.01°. Crystallographic refinement was carried out by simulating the XRD results using the Rietveld method, where the lattice parameter, cell volume and phase fractions were determined using Full Prof software. Crystallite size was calculated from XRD results using the Scherrer formula and Williamson-Hall (WH) Equation. The microstructure of the pellet surface was observed using a scanning electron microscope. Additionally, susceptibility and resistance measurements of the samples were carried out using the Lake Shore 7130 AC Susceptometer.

## 3. Results and discussion

Immediately after the heat treatment, equal sized pieces were cut from the samples and XRD measurements were carried out at room temperature by scanning the surface of these pieces between 20° and 90° with a step of 0.01°. In order to make a healthy comparison, XRD measurement results taken from equal surfaces were prepared with equal axis dimensions, Figure 1.

The expected impurity phase in $MgB_2$ is MgO resulting from the oxidation of metallic Mg [18-19]. At first glance, the samples except sample 625-06 appeared to be identical to pure $MgB_2$, with a trace of MgO as a second phase. As it is known, XRD patterns are observed as the sum of the reflections of all phases present in the sample, and the main peak of MgO at $2\theta \approx 42.8°$ is generally observed as a shouldered peak at the main peak of $MgB_2$. In this case, the reflection at $2\theta \approx 42.8°$ from MgO is not clearly observed because it is completely obscured by the main peak of $MgB_2$ originating from the (101) plane. On the other hand, the reflection of MgO at $2\theta \approx 63°$, corresponding to the (220) plane, which gives the second most intense peak, is clearly seen in all XRD patterns. While no other phase was observed in these five samples, in sample 625-06 it was determined that the main phase was Mg, the second phase was $MgB_2$ and the third phase was MgO. Accordingly, we can say that 6 hours of heat treatment at 625 °C is not sufficient in terms of time or process temperature for the reaction of all of the Mg used in the stoichiometric ratio in the in-situ synthesis of $MgB_2$. Moreover, when we compare this result with the 625C-12h and 650C-6h heat treatment results, it would be correct to say that only increasing the time or process temperature is sufficient for the Mg reaction to occur fully. As can be seen from the patterns shown using the same axis dimensions in Figure 1, the highest $MgB_2$ main peak was observed in the 650-06 sample and the lowest was observed in the 625-06 sample. If we accept that these measurements

are obtained from completely equal surfaces, we can say that processing at 650 °C creates more $MgB_2$ phase in both 6 hours and 12 hours of heat treatment compared to other temperatures. Moreover, if we evaluate it in terms of processing duration for each temperature, we can say that 6 hours of processing gives better results than 12 hours of processing. However, it should not be ignored that we assumed that the samples were divided into equal parts; there may have been minor differences in the surface dimensions of the cut samples.

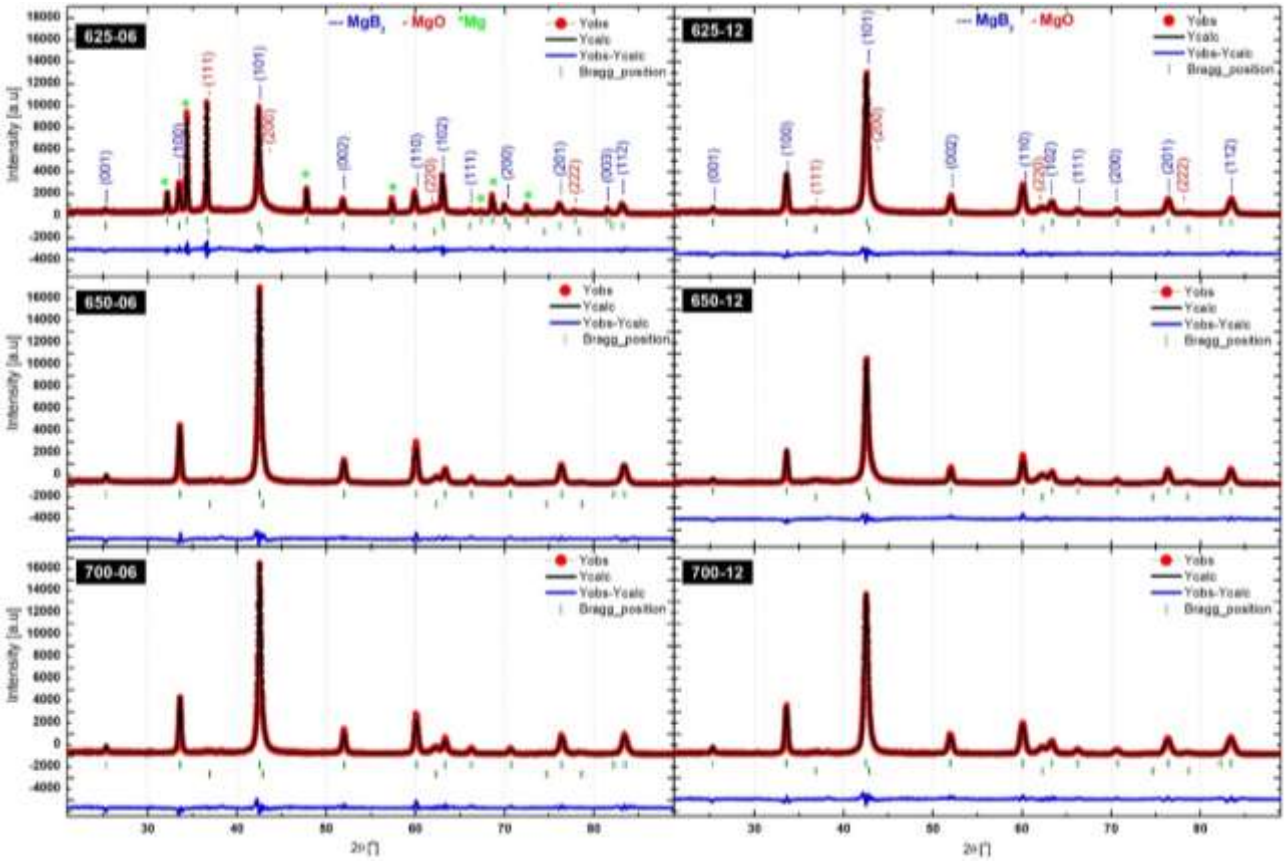


**Fig.1.** FullProf simulation of XRD patterns of produced samples

At this point, for a better comparison, the observed XRD patterns of the samples were multiphase refined with Reitveld to determine the volume fraction of MgO and the lattice parameters of the $MgB_2$ phase. For the refinement, firstly the phases were determined from the XRD pattern. Then, the average values of the required parameters of these phases were defined into the program in order to have a starting point for the refinement. The $MgB_2$ phase was defined as a member of the P6/mmm space group and the MgO phase was identified as a member of the Fm-3m space group. Background matching was first performed before starting to refine the XRD patterns of the produced samples. Pseudo-Voigt function was used to describe the peak shape. Then, the global parameters, scale factor, Caglioti parameters (U, V, W) and peak shape were improved, respectively. As the improvement was made gradually, the $\chi^2$ value which shows difference between the original measurement results and the patterns created by refinement showed a decrease. It was aimed to obtain the minimum $\chi^2$. Due to the presence of Mg, these refinements were made with 3 phases only in sample 625-06.

The difference between the original measurement results (red circles) and the calculated model (black line) is shown by the blue line. The Bragg reflections for MgB2 are shown by the green bars in the upper row and for MgO by the green bars in the lower row, Fig. 1. Table 1 shows the calculated lattice parameters of $MgB_2$ phase, and the calculated quantitative volume fraction of MgO in the samples by the Rietveld refinement.

When we examine Table 1, according to the phase percentages obtained as a result of refinement, the lowest MgO phase percentage was obtained in the 650-06 sample. Since Ar atmosphere is used in the heat treatment process, it is thought that the reason for the existence of the MgO phase is the oxidation of the samples prepared before the heat treatment and/or the purity of the rapidly oxidized Mg powder. The fact that the volume fraction of the MgO phase was limited to a maximum of 3% for all samples was interpreted as the samples being taken into XRD analysis immedialetly after the heat treatment without waiting. It has been observed that this proportional change, which occurs within a very small range, has no relationship with the heat

treatment temperature and duration. The relative density fraction of the MgO phase, which is one of the results obtained as a result of the multiphase Rietveld purification process, was calculated using the equation [20] for control purposes

$$D_{MgO}(\%) = \frac{I_{MgO(220)}}{\sum I_{MgB2(hkl)} + I_{MgO(220)}} \times 100$$

where *I* is the height of the XRD peak and (*hkl*) is the Miller indices. When the results calculated for each sample according to this formula were compared with the MgO fractions obtained as a result of Reitweld purification, it was observed that they showed a parallel trend, Fig. 2. It was thought that the difference observed only in sample 625-06 was due to the presence of a Mg phase, unlike the other five samples. According to both results, the lowest MgO phase ratio was observed in sample 650-06. Although it is a very small amount, it has been observed that generally an increase in temperature and time at 650 C and above causes an increase in the MgO ratio.

**Table 1:** Results of Rietveld refinement

| | ***Frac. of MgO*** | ***Lattice parameter of $MgB_2$*** |
|---|---|---|
| *625-06* | *0.14* | *a=b*=3.0868 Å, *c* =3.5251 Å |
| *625-12* | *1.44* | *a=b*=3.0789 Å, *c* =3.5156 Å |
| *650-06* | *1.05* | *a=b*=3.0797 Å, *c* =3.5171 Å |
| *650-12* | *2.99* | *a=b*=3.0802 Å, *c* =3.5172 Å |
| *700-06* | *1.33* | *a=b*=3.0780 Å, *c* =3.5167 Å |
| *700-12* | *1.28* | *a=b*=3.0800 Å, *c* =3.5185 Å |

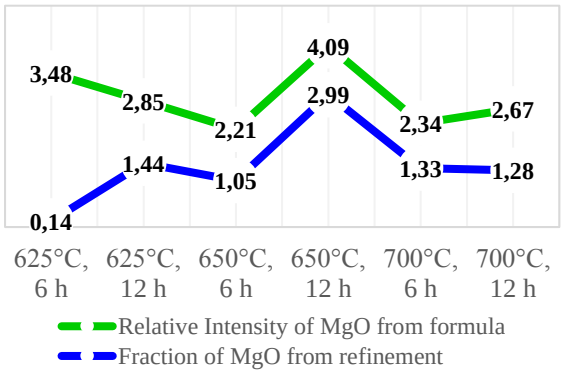


**Fig. 2.** Comparison of relative intensity of MgO from the formula and fraction of MgO phase from the FullProf

In addition, the crystal lattice parameters obtained as a result of the purification are given in the table and are in a range that can be considered compatible with the literature values. It is argued that a decrease in the a-lattice parameter indicates Mg deficiency [21]. The fact that they are slightly lower than the literature values can be interpreted as Mg deficiency occurring during heat treatment since excess Mg is not used. In terms of heat treatment temperature values and times, no identifiable trend was observed in the a and b-lattice parameters.

Another important parameter that determines the smoothness of the crystallographic structure is the width of the peaks. Multiphase Rietveld refinement of the samples revealed that MgO (200) peak, which we could not observe in the XRD pattern, is broader compared to the others in both 625 C samples. Same tendency was observed at (220) MgO peak. There are various contributions to the peak profile that forms XRD patterns, such as crystal size, microstrain, temperature and instrumental contributions. The Scherrer Equation, published in 1918 [22], relates the widths of XRD peaks only to the crystal size of the sample.

$$D = \frac{K\lambda}{\beta cos\theta}$$

where D is the size of crystallites, K is Scherrer constants (0.94) λ is the wavelength of Cu Kα radiation, β is FWHM of the peak, and θ is the peak position. The average crystallite size for the sample was calculated by taking the average of the crystallite sizes calculated with the Scherrer equation using the required values of selected $MgB_2$ peaks such as (100), (101), (002), (110), (201) and (112) in the XRD pattern. However, another issue to consider at this point is that the MgO (200) peak overlaps with the $MgB_2$ (101) peak. To exclude the contribution of MgO from the MgB2 peaks, calculations were made using the FWHM values obtained by the Rietveld refinement method from same peaks. As can be seen from Fig. 3, the average crystallite sizes obtained for each sample showed the same trend in the results obtained from both the XRD data and FullProf data. The difference between these two curves is thought to be the contribution of the MgO phase to the MgB2 peaks in the calculation made from the XRD peaks, because the curve using the FullProf results free of MgO contribution gave partially smaller results. Since sample 625-06 contains unreacted Mg phase, we can exclude this sample from evaluation as it is clearly observed from the XRD pattern that 625 C temperature and 6 h time are insufficient. We can say that no significant change in crystal size was observed until sample 700-12, and when it came to this sample, the crystallite size decreased.

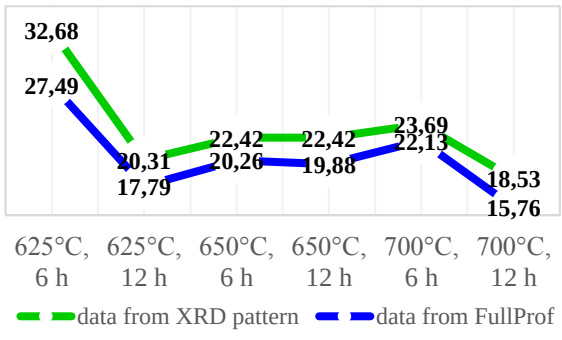


**Fig. 3.** Comparison of crystallite sizes calculated by Scherrer Equation using the XRD pattern and FullProf results

The Scherrer formula ignores the influence of strain on peak width. The Williamson-Hall Equation [23], which takes into account the microstrain that contributes to peak broadening as well as the crystal size, will provide more accurate results. For this purpose, the Williamson-Hall (WH) Equation combines the Scherrer equation, which determines the particle effect, and the Stokes-Wilson equation, which gives the micro stress, and is as follows:

$$\beta cos\theta = \frac{K\lambda}{D} + 4\varepsilon sin\theta$$

where β is the FWHM value of the peak (in radians) θ is the Bragg angle (in radians), K is the dimensionless Scherrer constant (0.94), λ is the wavelength of the X-ray source used (0.154056 nm), D is the crystal size (in nm), and ε is the lattice strain [24]. Ideally, when a graph is drawn by placing the term (4Sinθ) on the x-axis and the term (β.Cosθ) on the y-axis, a best line is drawn for the points obtained. While the slope of this line gives the intrinsic strain value, the point where it intersects the y-axis gives the average size of the crystals in the sample.

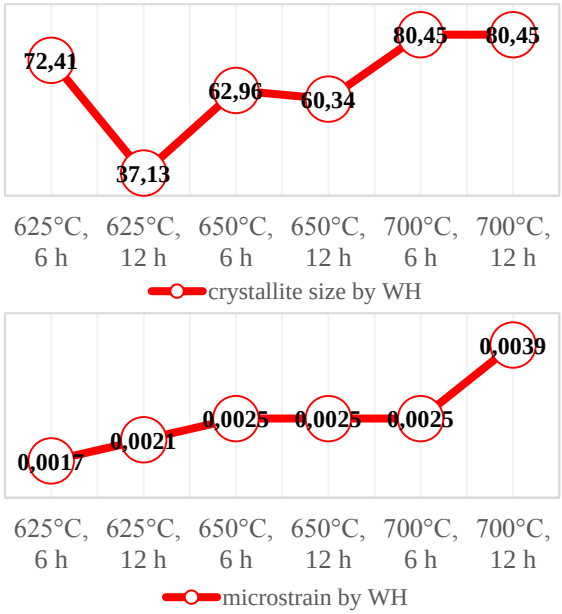


**Fig. 4.** Calculated crystallite size and microstrain by WH

When the crystallite size graphs in Fig3 and Fig4 are examined, it is seen that they have similar trends except for the 700-12 sample. We can say that the reason for this difference in the 700-12 sample is the Scherrer formula, which ignores the effect of strain on the peak width, and that there is a serious stress in this sample, as seen in Fig.4.

When we look at the crystallite sizes obtained from the WH equation (except sample 625-06), while the crystallite size increases with increasing temperature, there is almost no difference for different heat treatment duration at the same temperature. It is reported that the decrease in crystallite size will increase the scattering of electrons and therefore increase the upper critical field ($H_{c2}$) and resistivity value [25]. It has also been reported that decreasing the crystallite size reduces $T_c$ [26]. When evaluated from this perspective, we can say that it will create a situation that will negatively affect the critical current density ($J_c$) of the samples. In another study, from a different perspective, the improvement in $J_c$ was explained as the decrease in crystallite size improving the pinning mechanism [27]. Therefore, evaluating crystal size alone is not a sufficient criterion for transport properties. It is seen that the intrinsic strain values obtained from the WH equation are almost the same in samples 650-06, 650-12 and 700-06, but generally show an increasing trend with increasing temperature and time. In the 700-12 example, it showed a significant increase compared to the others.

SEM images taken from the surfaces of 12-hour heat treatment samples are shown in Figure 5. As seen from the SEM images, while the 625°C sample has a more porous and loose structure, fewer pores and a tighter structure are observed in the 650°C and 700°C samples.

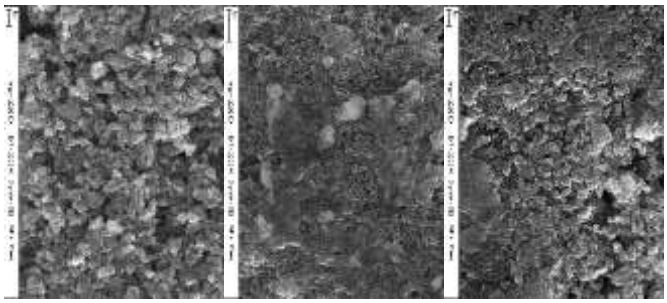

**Fig. 5.** SEM images of samples heat treated for 12 hours (from left to right: 625-12, 650-1, 700-12)

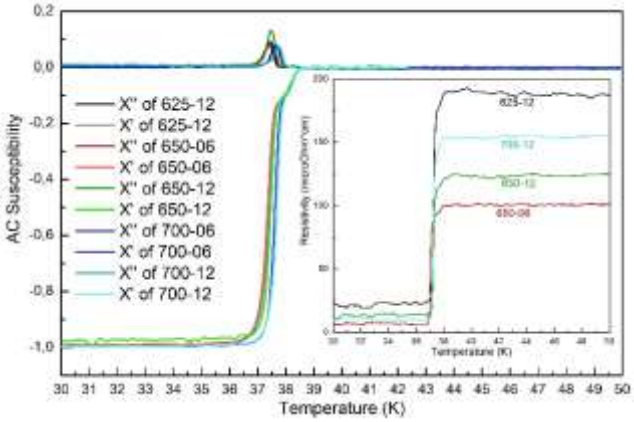


**Fig. 6.** AC susceptibility measurement results and inner graph shows resistivity measurement results

Susceptibility and resistance measurements of the samples were carried out using the Lake Shore 7130 AC Susceptometer. In the R(T) measurements taken with the help of the resistance apparatus of the AC Susceptometer, it was determined that all samples except the 625-06 sample showed a sharp transition at $T_c$ = 37,5 K. If we determine the

critical temperature $T_c$ in AC susceptibility measurements by defining it as the first deviation from the normal phase; we can say that all samples, except sample 625-06, exhibit the same characteristic transition at $T_{c,mag}$=38.5 K. In magnetic measurements taken from the samples, it was observed that grains exhibiting superconducting properties were formed around 38.5 K. However, the formation of a complete uninterrupted superconducting path trough the sample occurred around 37.5 K according to transport measurements. If the intervals in which the transition occurs are compared, we can say that the sharpest transition, although it does not bring a serious difference, is observed in the 700 C samples, and this sample is followed by the 650°C and 625 C samples in an expanding trend with small differences. These small differences are parallel to the crystal sizes. While a sharper transition and higher $T_c$ were observed in the 700-12 sample with larger crystal size, a slightly wider transition range and lower $T_c$ were obtained in the 650-12 sample with the smallest crystal size. According to magnetic measurements the effect of heat treatment duration was observed to be less than the effect of heat treatment temperature. When transport measurements were examined, heat treatment temperatures applied for 12 hours did not create a significant difference in the transition zone. On the other hand, according to the transport measurement results of the 650-06 and 650-12 samples, it was observed that the formation of the desired uninterrupted superconducting path in 6 hours shifted to lower temperatures. Considering the normal state resistances, we can say that 650 C shows lower resistance and offers a higher transport $T_c$ of 12 hours.

## 4. Conclusion

MgB2, which is an important candidate for the green technology of the future with its high transition temperature, has potential in areas such as portable applications, space applications requiring low-mass materials, transportation, medicine and energy, thanks to its light material. Therefore, in this study, we focused on MgB2 production by in-situ method for applications requiring high grain connectivity, as we believe that material properties should be evaluated and developed according to the needs of the applications. We examined the effects of production on the material at relatively low temperatures and times compared to the literature. According to the results we obtained from the XRD patterns, heat treatment at 625-650-700°C created only a 3% difference in the MgB2 phase ratio. The lattice parameters, which were consistent with the literatüre, there is no identifiable trend was observed in terms of heat treatment temperature values and times. The crystal size was found to increase with increasing temperature. Likewise, according to the results of transport and magnetic susceptibility measurements made with the AC susceptometer, no significant change in the critical temperature was observed with increasing temperature, while according to the transport measurement results, it was observed that the 12-hour period gave better results, although there was a small difference. As a result, we can say that lower temperatures can be tried depending on the needs of the application without making a big difference. In this way, it may be possible to reduce production costs.

## Acknowledgment

This work was supported by The Scientific and Technological Research Council of Türkiye-TUBITAK under the project number 121F272.

## References

[1] J. Nagamatsu, N. Nakagawa, T. Muranaka, Y. Zenitani ve J. Akimitsu, «Superconductivity at 39 K in magnesium diboride,» *Nature*, pp. 63-64, 2001.

[2] F. Cheng, Y. Liu, Z. Ma, H. Li ve M. S. A. Hossain, «Superior critical current density obtained in Mg 11 B 2 low activation superconductor by using reactive amorphous 11 B and optimizing sintering temperature,» *Journal of Alloys and Compounds*, cilt 650, pp. 508-513, 2015.

[3] S. X. Dou, O. Shcherbakova, W. K. Yeoh, J. H. Kim, S. Soltanian, X. L. Wang, C. Senatore, R. Flukiger, M. Dhalle, O. Husnjak ve E. Babic, «Mechanism of Enhancement in Electromagnetic Properties of MgB2 by Nano SiC Doping,» *PHYSICAL REVIEW LETTERS*, cilt 98, no. 9-2, pp. 097002-1-4, 2007.

[4] Z. Gao, Y. Ma, X. Zhang, D. Wang, H. Yang, H. Wen ve K. Watanabe, «Influence of oxygen contents of carbohydrate dopants on connectivity and critical current density in MgB2 tapes,» *Applied Physics Letters*, cilt 91, no. 16, p. 162504, 2007.

[5] M. S. A. Hossain, A. Motaman, X. Xun, K. W. See, Ö. Çiçek, H. Ağıl, E. Ertekin, A. Gencer, K. Cheong, M. Maeda ve S. X. Dou, «Structurally homogeneous MgB2 superconducting wires through economical wet mixing process,» *Materials Letters*, cilt 91, pp. 356-358, 2013.

[6] G. Giunchi, S. Raineri, R. Wesche ve P. L. Bruzzone, «The voltage–current relations for MgB2 obtained by reactive liquid infiltration,» *Physica C: Superconductivity*, cilt 401, no. 1-4, pp. 310-315, 2004.

[7] G. Giunchi, G. Ripamonti, T. Cavallin ve E. Bassani, «The reactive liquid Mg infiltration process to produce large superconducting bulk MgB2 manufacts,» *Cryogenics*, cilt 46, no. 2-3, pp. 237-242, 2006.

[8] A. Bhagurkar, «Processing of MgB2 Bulk Superconductor by Infiltration and Growth,» Brunel Univeristy London, London, 2017.

[9] V. Braccini, D. Nardelli, R. Penco ve G. Grasso, «Development of ex situ processed MgB2 wires and their applications to magnets,» *Physica C: Superconductivity,* cilt 456, no. 1-2, p. 209–217, 2007.

[10] A. Serquis, L. Civale, J. Y. Coulter, D. L. Hammon, X. Z. Liao, Y. T. Zhu, D. E. Peterson, F. M. Mueller, V. F. Nesterenko ve S. S. Indrakanti, «Large field generation with a hot isostatically pressed powder-in-tube MgB2coil at 25 K,» *Superconductor Science and Technology,* cilt 17, no. 10, pp. L35-L37, 2004.

[11] K. Vinod, N. Varghese ve U. Syamaprasad, «Superconductivity of MgB2 in the BCS framework with emphasis on extrinsic effects on critical temperature,» *Superconductor Science and Technology,* cilt 20, no. 10, pp. R31-R45, 2007.

[12] D. Mijatovic, A. Brinkman, D. Veldhuis, H. Hilgenkamp, H. Rogalla, G. Rijnders, D. H. A. Blank, A. V. Pogrebnyakov, J. M. Redwing, S. Y. Xu ve X. X. Xi, «SQUID magnetometer operating at 37 K based on nanobridges in epitaxial MgB2 thin films,» *Applied Physics Letters,* cilt 87, no. 19, pp. 192505-1-3, 2005.

[13] S. A. Cybart, K. Chen, Y. Cui, Q. Li, X. X. Xi ve R. C. Dynes, «Planar MgB2 Josephson junctions and series arrays via nanolithography and ion damage,» *Applied Physics Letters,* cilt 88, no. 1, pp. 012509-1-2, 2006.

[14] K. Chen, Y. Cui, Q. Li, X. X. Xi, S. A. Cybart, R. C. Dynes, X. Weng, E. C. Dickey ve J. M. Redwing, «Planar MgB2 superconductor-normal metal-superconductor Josephson junctions fabricated using epitaxial MgB2/TiB2 bilayers,» *Applied Physics Letters,* cilt 88, no. 22, pp. 222511-1, 2006.

[15] A. Yamamoto, A. Ishihara, M. Tomita ve K. Kishio, «Permanent magnet with MgB2 bulk superconductor,» *Applied Physics Letters,* cilt 105, no. 3, p. 032601, 2014.

[16] H. Kobayashi, M. Muralidhar, M. R. Koblischka, K. Inoue ve M. Murakami, «Improvement in the Performance of Bulk MgB2 Material through Optimization of Sintering Process,» *Physics Procedia,* cilt 65, pp. 73-76, 2015.

[17] L. Yang, H. Suo, L. Ma, M. Liu, Y. Dai, J. Cheng, Z. Zhang ve Q. Wang, «A novel sintering protocol to enhance the connectivity of ex situ MgB2 bulks in an open system by using Mg vapor,» *Superconductor Science and Technology,* cilt 33, no. 4, pp. 1-7, 2020.

[18] G. Alecu, A. Cosac ve S. Zamfir, «Superconductivity in MgB2,» *Annals of the University of Craiova. Electrical Engineering Series,* cilt 30, pp. 382-385, 2006.

[19] N. Varghese, K. Vinod, A. Rao, Y. K. Kuo ve U. Syamaprasad, «Enhanced superconducting properties of bulk MgB2 prepared by in situ Powder-In-Sealed-Tube method,» *Journal of Alloys and Compounds,* cilt 470, no. 1-2, pp. 63-66, 2009.

[20] J. H. Kim, S. X. Dou, M. Rindfleisch ve M. Tomsic, «Study of MgO formation and structural defects in in situ processed MgB2,» *Superconductor Science and Technology,* cilt 20, no. 10, pp. 1026-1031, 2007.

[21] C. H. Jiang ve H. Kumakura, «Stoichiometry dependence of the critical current density in pure and nano-SiC doped MgB2/Fe tapes,» *Physica C: Superconductivity,* cilt 451, no. 1, pp. 71-76, 2007.

[22] P. Scherrer, «Bestimmung der Grösse und der inneren Struktur von Kolloidteilchen mittels Röntgenstrahlen,» *Nachr. Ges. Wiss. Göttingen,* cilt 26, pp. 98-100, 1918.

[23] G. K. Williamson ve W. H. Hall, «X-ray line broadening from filed aluminium and wolfram,» *Acta Metallurgica,* cilt 1, no. 1, pp. 22-31, 1953.

[24] H. Durmuş ve K. Kocabaş, «The influence of Mn nanoparticles on superconducting properties and pinning mechanism of MgB2,» *Journal of Materials Science: Materials in Electronics,* cilt 33, pp. 17079-17089, 2022.

[25] C. Tarantini, H. U. Aebersold, V. Braccini, G. Celentano, C. Ferdeghini, V. Ferrando, U. Gambardella, F. Gatti, E. Lehmann, P. Manfrinetti, D. Marre, A. Pelenzona, I. Pallecchi, I. Sheikin, A. S. Siri ve M. Putti, «Effects of neutron irradiation on polycrystalline Mg11B2,» *Phys. Rev. B,* cilt 73, p. 134518, 2006.

[26] B. Lorenz, O. Perner, J. Eckert ve C. W. Chu, «Superconducting properties of nanocrystalline MgB2,» *Supercond. Sci. Technol.,* cilt 19, pp. 912-915, 2006.

[27] H. Fuji ve H. Kitaguchi, «Superconducting properties of sintered ex situ MgB2 tapes through ball milling process as a function of crystallite size in the as-milled and sintered states,» *Physica C: Superconductivity and its Applications,* cilt 583, p. 1353838, 2021.